

Fluorination of an Alumina Surface: Modeling Aluminum–Fluorine Reaction Mechanisms

Richa Padhye,[†] Adelia J. A. Aquino,^{*,‡,§,||} Daniel Tunega,[§] and Michelle L. Pantoya^{*,†}

[†]Department of Mechanical Engineering and [‡]Department of Chemistry and Biochemistry, Texas Tech University, Lubbock, Texas 79409, United States

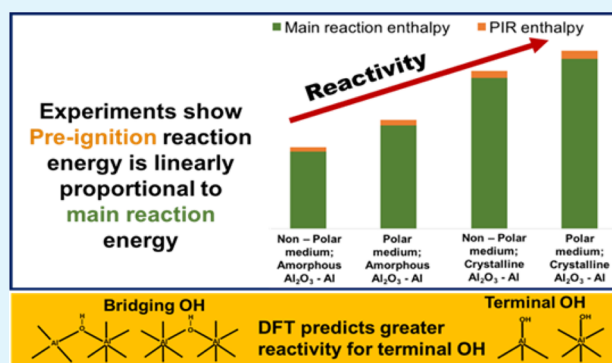
[§]Institute for Soil Research, University of Natural Resources and Life Sciences, Peter-Jordan-Strasse 82, A-1190 Vienna, Austria

^{||}School of Pharmaceutical Sciences and Technology, Tianjin University, Tianjin 300072, P. R. China

Supporting Information

ABSTRACT: Density functional theory (DFT) calculations were performed to examine exothermic surface chemistry between alumina and four fluorinated, fragmented molecules representing species from decomposing fluoropolymers: F⁻, HF, CH₃F, and CF₄. The analysis has strong implications for the reactivity of aluminum (Al) particles passivated by an alumina shell. It was hypothesized that the alumina surface structure could be transformed due to hydrogen bonding effects from the environment that promote surface reactions with fluorinated species. In this study, the alumina surface was analyzed using model clusters as isolated systems embedded in a polar environment (i.e., acetone). The conductor-like screening model (COSMO) was used to mimic environmental effects on the alumina surface. Four defect models for specific active –OH sites were investigated including two terminal hydroxyl groups and two hydroxyl bridge groups. Reactions involving terminal bonds produce more energy than bridge bonds. Also, surface exothermic reactions between terminal –OH bonds and fluorinated species produce energy in decreasing order with the following reactant species: CF₄ > HF > CH₃F. Additionally, experiments were performed on aluminum powders using thermal equilibrium analysis techniques that complement the calculations. Consistently, the experimental results show a linear relationship between surface exothermic reactions and the main fluorination reaction for Al powders. These results connect molecular level reaction kinetics to macroscopic measurements of surface energy and show that optimizing energy available in surface reactions linearly correlates to maximizing energy in the main reaction.

KEYWORDS: DFT calculations, modified alumina structures, implicit solvent model, alumina, catalysis, fluoropolymer reactions, aluminum combustion, fluorides



INTRODUCTION

The science of aluminum fuel particle reactivity with fluoropolymers has important implications toward new processing techniques in the additive manufacturing of energetic materials. Many binders used in energetic composites, such as Kel-F and Viton,¹ as well as poly(vinylidene fluoride) (PVDF),² contain fluorine and are processed with aluminum fuel powder for the purpose of creating tailorable architectures. The reactivity of aluminum with fluorinated materials is therefore becoming an important area of research toward advancing energetic material science from a processing as well as a combustion perspective.

The aluminum powder used in aluminum/fluorine composites is composed of Al particles that have a core–shell structure. The core of the Al particle is crystalline Al, and the shell is amorphous Al₂O₃.³ The Al₂O₃ shell surrounding the crystalline Al core acts as an oxygen diffusion barrier, limiting the oxidation of crystalline Al.⁴ In traditional Al combustion,

the Al₂O₃ shell is inert (i.e., does not chemically react to produce heat) and absorbs heat (i.e., acts as a heat sink). Recently, the inert oxide shell has been shown to have potential for contributing to the overall energy generated in Al combustion by utilizing an exothermic reaction between fluorine and Al₂O₃. Osborne et al.⁵ showed that the alumina shell on an aluminum particle reacts with fluorinated species from a decomposing fluoropolymer, producing an exothermic surface reaction that also facilitates decomposition of the fluoropolymer. The surface reaction occurs prior to the main aluminum fluorination reaction and is referred to as a “preignition reaction” or PIR.⁵ Pantoya and Dean⁶ further showed that the surface area exposure of alumina and the fluoropolymer is directly related to the amount of energy

Received: April 17, 2017

Accepted: June 28, 2017

Published: June 28, 2017

generated in the PIR and showed that the β - to α -AlF₃ phase transition is not only exothermic but also occurs at the same temperature as the main Al fluorination reaction. Therefore, the surface chemistry producing an exothermic PIR also contributes to the main reaction via exothermic AlF₃ phase transitions coinciding with the aluminum fluorination reaction. Therefore, there are two energy benefits from the surface reaction between fluorinated species and alumina: (1) the PIR and (2) exothermic AlF₃ phase transition coinciding with energy generation from the main reaction of the Al core.

The thickness of the Al₂O₃ shell is independent of particle size. Therefore, nanoscale Al particles have greater concentration of Al₂O₃ per volume than micron-scale Al particles. The reduced surface area to volume ratio in micron-scale particles has limited detection of PIRs to nanoscale Al particles. More recently, exothermic reactions between fluorine and the aluminum oxide shell were exploited for engineering more reactive aluminum composites using micron-scale aluminum particles.^{7,8} McCollum et al. used a liquid fluoro-oligomer, perfluoropolyether (PFPE) that wetted and coated the surface of micron-scale aluminum particles.^{9,10} They showed that the intimate contact between fluoropolymer and the alumina surface induced a PIR that also enhanced the reactivity of the Al–PFPE composite particle with a metal oxide, molybdenum trioxide (MoO₃). Increasing PFPE concentration corresponded to an increase in PIR and a main exothermic reaction and also corresponded to a proportional increase in flame speed. In fact, they also showed that PFPE-coated micron-scale Al particles produced a PIR, and that was the first time a PIR had been observed with micron-scale Al particles.

Fluorination reactions with crystalline phases of alumina have been studied for applications beyond energetic materials and toward the microelectronics industry for cleaning and etching aluminum-containing materials. These studies have some relevance here and will be discussed in brief. King et al.¹¹ and Shamiryani et al.¹² reviewed numerous areas where fluorine interactions with Al and Al₂O₃ are relevant because the high dielectric constant of Al₂O₃ makes it an appealing alternative to SiO₂ substrates for downsizing the electronic base. Thus, the wet and dry (plasma) chemistry required to selectively remove alumina (i.e., etching) has led to the identification of key chemical interactions that also have importance to energetic material applications. For example, Dhungana et al.¹³ specifically investigated etching of Al₂O₃ using CF₄ and CHF₃ chemistries, and their findings show high etch rates for these chemistries and the feasibility for multipattern optical lithography processing.

Because our goal is to exploit fluorine-based surface reactions with alumina toward heightened reactivity, early studies such as by Zivkovic et al.¹⁴ also provide context for the exothermic nature of fluorination reactions. Zivkovic et al.¹⁴ showed that fluorine interactions with alumina can reduce the onset temperature for exothermic crystallization of alumina by 200 °C. Their finding was from a thermal equilibrium analysis (i.e., differential scanning calorimetry, DSC) that showed AlF₃ acts as a catalyst promoting early onset of exothermic surface chemistry. Deshumkh et al.¹⁵ examined FTIR spectra on the interaction of CF₃CFCl₂ with Al₂O₃ to show surface absorption of F at nearly room-temperature conditions, indicating a low activation energy for fluorination reactions with Al₂O₃. The stability of AlF₃ in the presence of H₂O has also been studied to show that environmental conditions play a strong role in surface bonding related to exothermic fluorination reactions.

Bailey et al. showed that the formation of hydrogen bonds between the OH[−], HF, and H₂O species to nearby F and O ions occurs readily, but the stable surfaces always maximize such bonding.^{16,17} These findings have particular relevance to energetic materials where the processing environment may be polar or nonpolar, thereby introducing unique hydrogen bonding that will influence fluorination of the surface.

All of these studies suggest that there is still room to exploit the potential to enhance Al reactivity, especially toward transitioning reactivity enhancements seen in nanoscale Al powder toward micron-scale Al powder. The goal of this study is to further understand surface reactions between alumina and fluorinated species from decomposing fragments of fluoropolymers. Not only will this understanding contribute toward new strategies to functionalize aluminum particles toward greater reactivity but also the fundamental kinetics may be applied to fuel particles with oxide shells that may produce reactions similar to alumina, such as oxides of magnesium, boron, and silicon.^{18–20}

As a first step toward this goal, first-principle density functional theory (DFT) calculations were performed on five alumina clusters mimicking different surface hydroxyl sites.²¹ It was observed that when surrounded by a strongly electro-negative polar environment the surface alumina structure is affected by hydrogen bonding forces differently than the same interface not treated by a polar environment. Specifically, the overall hydroxyl bond distances increase; the surface charge increases; and vibrational frequencies decrease. These surface modifications are linked to greater surface reactivity of aluminum particles with alumina shells that are processed using a polar solvent than the same powder processed using a nonpolar solvent.^{21,22}

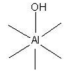
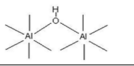
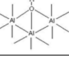
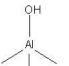
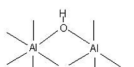
As a check on these computational results, thermal equilibrium and flame speed studies were performed with aluminum powder treated in polar and nonpolar solvents.²² The results showed three interesting observations: (1) energy generated during the preignition reaction (PIR) was linearly proportional to energy generated in the main reaction; (2) higher energy generated during the PIR and main reaction was directly proportional to higher flame speeds; and (3) aluminum particles treated in polar solvents consistently showed greater PIR and main reaction exotherms as well as a 3-fold increase in flame speed compared with aluminum particles treated in nonpolar solvents.²² These results coupled with the model results from ref 14 suggest irreversible surface modifications caused by polar environments.

The following study intends to create a bridge between experiments and molecular modeling calculations. The objective is to model exothermic surface reactions on an alumina surface exposed to a single fluorinated species that replaces a surface hydroxyl group bound to an aluminum atom. Four different Al coordinations representing hydroxyl reactive sites are simulated using molecular clusters up to 130 atoms. For each cluster, two environments are investigated representing surface treatment in a polar solvent versus an untreated surface that is exposed to an ambient environment. The calculations were performed using density functional theory (DFT) method. The model was developed to examine elementary reactions that promote exothermic surface energy and how those reactions are affected by surface treatment and temperature. An additional objective is to complement these calculations with an experimental equilibrium study of Al powder treated in a polar versus nonpolar environment.

Because the DFT method assumes a crystalline alumina surface but an amorphous alumina surface comprises Al particles, experiments were also performed for Al powder with both crystalline and amorphous alumina surfaces. In this way, the applicability of the DFT results to experimental observations could be assessed.

Density Functional Theory Calculations. The alumina shell of the aluminum particles is assumed to consist of several surface hydroxyl sites similar to those defined by Peri²³ and by Knözinger and Ratnasamy²⁴ for crystalline alumina phases. Previously, Padhye et al.²¹ constructed cluster models for five different OH sites known for the surfaces of the γ -Al₂O₃ phase. In these models (Table 1) two sites represent terminal –OH

Table 1. Notation for Five γ -Al₂O₃ Surface Hydroxyl Coordinations That Correspond to Various References Indicated^a

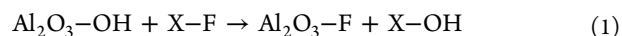
Padhye ¹⁴	Peri ¹⁶	Knözinger and Ratnasamy ¹⁷	Model
I	A	Ib	
II	B	IIb	
III	C	III	
IV	D	Ia	
V	E	IIa	

^aThe notation taken in this study corresponds with Padhye et al.¹⁴

groups linked to one Al atom (one in octahedral and one in tetrahedral coordination, models I and IV); two sites represent bridged –OH groups (bound to two Al atoms, models II and V); and one site represents an –OH group connected to three Al atoms (model III). Dangling Al–O bonds on the edges and surface oxygen atoms were saturated by hydrogen atoms in a way to ensure an overall zero charge for the final cluster structure (total amount of atoms extended to 110–130 atoms). To preserve structural features of the γ -Al₂O₃ surface, partial geometry optimization was performed in two steps. First, all hydrogen atoms were relaxed while the oxygen and aluminum atoms were frozen. Then, oxygen and hydrogen atoms of the surface OH groups plus aluminum atoms bonded to the

particular –OH site and a few oxygen atoms around were relaxed; all remaining atoms stayed frozen. Then, properties of the five OH sites were analyzed (structure, charges, H-bonding, and OH stretching frequencies).¹⁴

Surface fluorination reaction mechanisms are complex, but as a first step, elementary exchange reactions are considered in which OH[–] is replaced with F[–] as described in eq 1, where X–F is a fluorine-bearing moiety.



In this reaction the Al–O bond is breaking, and the Al–F bond is forming. Our models have four different hydroxyl coordinations: sites I, II, IV, and V. In Table 1, site III has three Al atoms bound to the hydroxyl group, and the chemical breaking of the three Al–O bonds is energetically very demanding. Therefore, this model was excluded from the calculation of the reaction energies according to eq 1. In the remaining four clusters the central –OH group was replaced by F atoms (see Figure 1), and such fluorinated structures were optimized using the same geometry constraints as in the optimization of the original clusters described before. The following fluorinated species were used as model X–F structures: pure F[–] ion, HF, CH₃F, and CF₄. We note that the exchange reaction with F[–] is unrealistic but is included to show a hierarchical set of F[–] species with corresponding results confirming this reaction is not realistic. Also, DeLisio et al. observed that for poly(vinylidene fluoride) (PVDF) reacting with Al particles oxidation takes place due to the production of hydrofluoric (HF) gas when PVDF decomposes.⁸ For this reason, HF was included in the X–F structures. As mentioned previously, Dhungana et al.¹³ identified CH₃F and CF₄ chemistries as uniquely poised for high etch rates for Al₂O₃ and thus merits investigation here too. To complete the reaction scheme (eq 1) the calculations were also carried out to OH[–], H₂O, CH₃OH, and CF₃OH structures as reaction products, respectively.

The calculations were performed at the same DFT level as used in ref 21 (Becke–Perdew (B–P) functional^{25–29} and a split-valence polarization (SVP) basis set³⁰). Two different environments for the fluorination reaction (eq 1) were considered in the computations: nonpolar (representing ambient) and polar (representing acetone with a relative dielectric constant, $\epsilon_r = 20.70$ ³¹). For the latter the conductor-like screening model (COSMO³²) was used. The ambient condition refers to the alumina surface that has not been treated with a polar solvent. Moreover, for the gas-phase condition thermochemistry calculations were performed for a set of different temperatures ranging from room temperature to 600 K. It is noted that the reactions in the polar environment

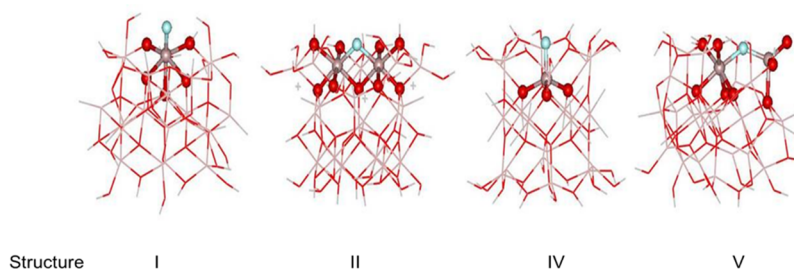


Figure 1. Structures of four cluster models with structure label corresponding to sites shown in Table 1. Reaction sites are in a ball-and-stick mode: oxygen atoms in red, fluorine atoms in light blue, and aluminum atoms in tan color.

are hypothetical and representative of the alumina surface treated in a polar fluid. The Turbomole program suite³³ was used to perform all calculations.

EXPERIMENTAL SECTION

The calculations assume the alumina surface is in a γ - Al_2O_3 crystalline phase. However, the alumina layer surrounding the aluminum core particle is amorphous. Therefore, the applicability of the DFT results toward actual applications with aluminum particles is investigated here by transforming the amorphous passivation shell into a crystalline phase. In this study, aluminum particles were supplied by NovaCentrix (Austin, TX) and are characterized using a transmission electron microscope (TEM), Brunauer–Emmett–Teller (BET) theory, and dynamic light scattering to be on average 80 nm in diameter with a 2–3 nm thick passivation shell.²² Transitioning the alumina phase is accomplished by heating the powder in a Fisher Scientific Isotemp model 281A Vacuum Oven, manufactured by Thermo Fisher Scientific to 450 °C for 15 min under vacuum. The amorphous to crystalline phase transition for alumina is 440 °C.³⁴ This heating protocol was found to be the minimum time to (1) transition the shell from amorphous to crystalline γ - Al_2O_3 while (2) not growing the thickness of the shell appreciably and therefore consuming the aluminum core. In this way, reactivity of aluminum particles with an amorphous compared with a crystalline shell could be investigated without the additional influence of the variable shell thickness (and oxidized aluminum core). Work by Gesner et al. helped establish this heating protocol.³⁵ Figures S1 A and B show TEM images of an Al particle before and after the prescribed heat treatment.

Shell crystallization to γ - Al_2O_3 was confirmed through X-ray diffraction (Figure S2). A fully automated, high precision Siemens/Bruker D5005 Theta/2 Theta Bragg–Brentano diffractometer was used to detect the presence of γ - Al_2O_3 . The equipment uses a 2.2 kW sealed Cu X-ray source, a high-precision vertical Theta/2 Theta goniometer, standard sample stage, curved graphite crystal diffracted beam monochromator, and NaI(Tl) scintillation counter detector. Figure S2 shows the XRD data indicating amorphous to crystalline phase transition after thermal treatment.

Aluminum particles with crystalline or amorphous alumina shells were combined with PTFE particles supplied by DuPont (Wilmington, DE) as Zonyl MP 1400. The PTFE particles are 10 μm average diameter. The powders were mixed to a 1.5 equivalence ratio such that each powder mixture prepared was approximately 500 mg and suspended in either a nonpolar solvent, hexane (supplied by Fisher Chemical, reagent grade or better with negligible water concentration measured by Karl Fisher Titration), or a polar solvent, acetone (supplied by Fisher Chemical, reagent grade or better with 0.8% vol. water concentration measured by Karl Fisher Titration). The hexane (nonpolar) or acetone (polar) acts as the carrier fluid aiding intermixing of the fuel and oxidizer particles. The solid to liquid ratio is constant and 500 mg:60 mL and contained in a 120 mL vial that is sonicated using a Misonix Sonicator 3000 (Farmingdale, NY). Sonication helps break up agglomerates and improve homogeneity and is programmed on a 10 s on/off cycle to prevent solution heating. The mixture is poured into a Pyrex dish and the hexane or acetone allowed to evaporate in the fume hood in ambient conditions for 24 h. Powder mixtures were reclaimed for further experimentation. It is noted that without a carrier fluid the fuel and oxidizer particles do not mix well enough to produce a homogeneous dispersion that will provide repeatable results. For example, Padhye et al.²² showed that Al + PTFE dry mixed (i.e., mixed with no carrier fluid) would not produce surface reactions (i.e., see Figure 3 in ref 22), and the main oxidation reaction was shifted to a higher onset temperature by 50 °C with significantly reduced reaction energy (see Figure 4 in ref 22). They also provide SEM with EDS images that show the degree of dispersion using polar (acetone or isopropanol) versus nonpolar (hexane) is about equal, such that mixture homogeneity between the two carrier fluids does not account for the differences in reactivity observed.²²

A Netzsch Jupiter simultaneous thermal analyzer (STA) 449 differential scanning calorimeter (DSC) was used for thermal

equilibrium analysis. About 5–7 mg mixtures were loaded into alumina crucibles and into an automated sample holder. All experiments were carried out from 45 to 1000 °C and were triplicated to evaluate repeatability. All mixtures were analyzed at a heating rate of 5 °C/min under argon/oxygen environment (i.e., 80 vol % Ar/20 vol % O_2).

RESULTS

Theoretical Calculations. The results of calculated reaction energies, ΔE_r (eq 1), for four reaction –OH sites (i.e., sites I, II, V, IV in Table 1) in nonpolar and polar environments are shown in Figure 2(a)–(d), and the

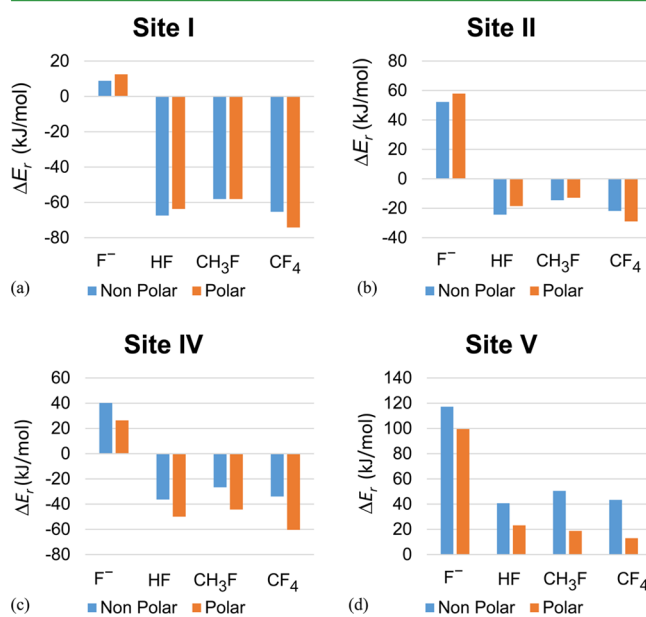


Figure 2. Calculated reaction energy (ΔE_r , kJ/mol) for (a) hydroxyl octahedral terminal coordination, $\text{Al}_\text{O}-\text{OH}$ (site I); (b) hydroxyl octahedral bridging coordination, $\text{Al}_\text{O}-\text{OH}-\text{Al}_\text{O}$ (site II), (c) hydroxyl tetrahedral terminal coordination, $\text{Al}_\text{T}-\text{OH}$ (site IV), and (d) hydroxyl bridging OH linked to one Al in octahedral and one Al in tetrahedral coordination, $\text{Al}_\text{O}-\text{OH}-\text{Al}_\text{T}$ (site V).

corresponding data are tabulated in Supporting Information, Table S1. Figure 1 corresponds to optimized geometries of the cluster models with the fluorinated $\text{Al}_2\text{O}_3-\text{F}$ sites. The nonpolar environment used in the calculations corresponds to the ambient condition referring to the alumina surface that has not been treated with a polar solvent, while the polar environment refers to the alumina surface that has been treated with a polar solvent. The experimental corollary to the ambient condition used hexane as the carrier fluid to mix Al + PTFE powders. The polar condition is simulated experimentally by using acetone as the carrier fluid to mix Al + PTFE. It is noted that acetone was measured to have 0.8 vol % water concentration.

Figure 3 graphically represents the changes in Gibbs free energy, ΔG_r (eq 1), at ambient and elevated temperatures. The calculations were performed for the nonpolar conditions only. The corresponding data are tabulated in Table S2 of Supporting Information. Table S2 also contains calculated reaction enthalpies, ΔH_r .

Experiments. Information from the differential scanning calorimetry (DSC) and thermal gravimetric (TG) analyses is presented in Figure 4 for aluminum powder that contained either an amorphous or crystalline shell and was treated in

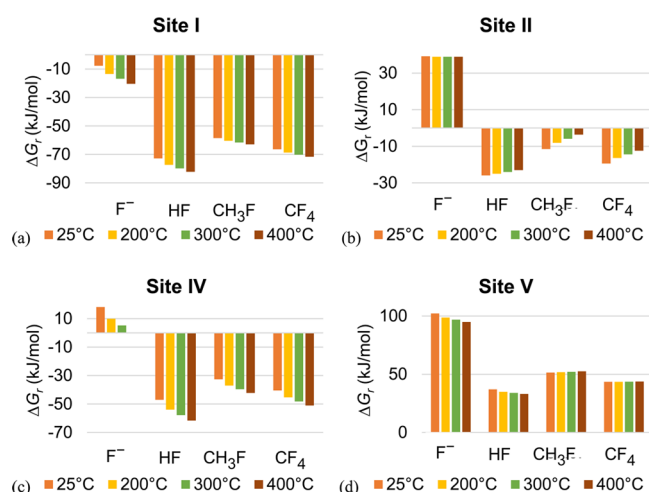


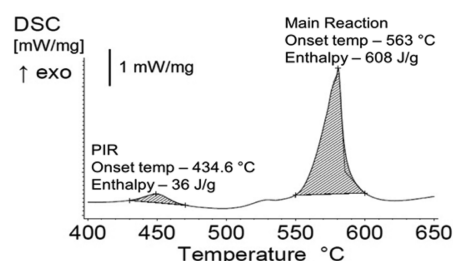
Figure 3. Calculated reaction Gibbs free energy (ΔG_r , kJ/mol) according to eq 1 species at four different temperatures for (a) hydroxyl octahedral terminal coordination, Al_O-OH (site I); (b) hydroxyl octahedral bridging coordination, $Al_O-OH-Al_O$ (site II); (c) hydroxyl tetrahedral terminal coordination, Al_T-OH (site IV), and (d) hydroxyl bridging OH linked to one Al in octahedral and one Al in tetrahedral coordination, $Al_O-OH-Al_T$ (site V).

either a polar or nonpolar environment. Figures 4(a–d) show that a PIR exists for Al powder with passivation shells that are amorphous or crystalline. The onset temperature and exothermic enthalpy of reaction from the DSC analysis in Figure 4 are tabulated in Table 2. The crystalline shell demonstrates a reduced onset for the PIR (i.e., 426–428 °C for crystalline shell and 432–434 °C for amorphous) as well as an increased enthalpy of reaction for both fluid treatments (i.e., 56 and 64 mJ/mg for a crystalline shell compared with 36 and 42 mJ/mg for an amorphous shell). In general, Table 2 shows that surface exothermic reactions on Al powders with crystalline shells are greater than for the same powder with an amorphous shell. Also, for either crystalline or amorphous shells, treatment in a polar fluid reduces the onset temperature and increases the energy from the surface exothermic reaction compared to nonpolar fluid processing. The results for the PIR in Table 2 indicate the DFT calculation assumption that the particle passivation shell is crystalline and does not significantly affect predictions for surface exothermic reactions in Al particles but is an upper limit approximation for Al powder with amorphous passivation shells.

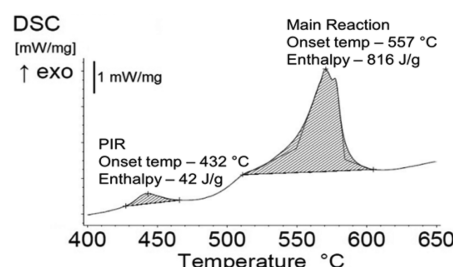
Regarding the main reaction, the Al powder with crystalline shells consistently produces lower onset temperatures (i.e., by 50 degrees for polar processing fluid and 13 degrees for nonpolar processing fluid) and greater enthalpies for both polar and nonpolar fluid treatments (i.e., 1186 and 1340 mJ/mg for crystalline compared with 608 and 816 mJ/mg for amorphous shells). These results suggest $\gamma-Al_2O_3$ contains more active sites than amorphous Al_2O_3 , leading to greater surface reactivity.

DISCUSSION

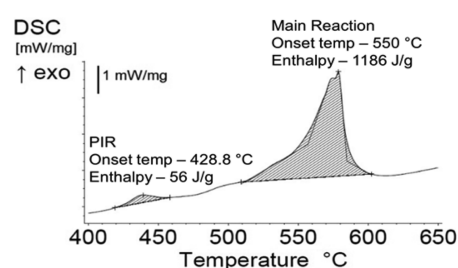
Figure 2 shows that the most energetically favorable reactions occur at the terminal hydroxyl coordinations (i.e., octahedral, Site I; and, tetrahedral, Site IV, Al coordination). The largest energetic gain for both terminal coordinations occurs with CF_4 and HF, followed by CH_3F . There is a difference in calculated reaction energy for the polar compared to the nonpolar condition. For the octahedral hydroxyl coordination (site I),



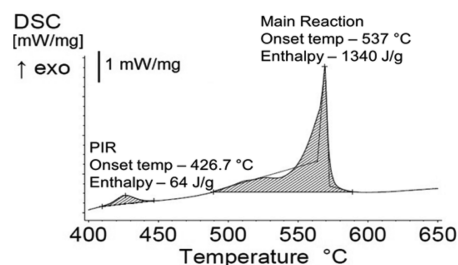
(a) Amorphous alumina shell treated in a nonpolar environment.



(b) Amorphous alumina shell treated in a polar environments.



(c) Crystalline $\gamma-Al_2O_3$ shell treated in a nonpolar environment.



(d) Crystalline $\gamma-Al_2O_3$ shell treated in a polar environment.

Figure 4. DSC data for heat flow as a function of temperature for Al combined with PTFE. (a) Al powder with an amorphous alumina shell treated in a nonpolar environment. (b) Al powder with an amorphous alumina shell treated in a polar environment. (c) Al powder with a crystalline $\gamma-Al_2O_3$ shell treated in a nonpolar environment. (d) Al powder with a crystalline $\gamma-Al_2O_3$ shell treated in a polar environment. Heating rate is 5 °C/min under 80 vol % argon/20 vol % oxygen. Shaded areas correspond to enthalpy shown in Table 2.

the nonpolar environment incites a slightly higher reaction energy (except CF_4 , Table S1). For the tetrahedral hydroxyl coordination (site IV), the changes are more significant, and the polar environment enhances the energetic gain. However, the magnitude of the reaction energy associated with all reactions at site I is greater than the corresponding reactions at site IV, implying site I is the most reactive site.

Figure 3 shows the change in Gibbs free energy for each reaction according to eq 1 and hydroxyl coordinations shown in Figure 1. Surface reactions at sites I, II, and IV are exergonic with exception for the reactions with F^- for sites II and IV that are endergonic, while at site V, all reactions are endergonic.

Table 2. Values for the Onset Temperature and Reaction Enthalpy from DSC Data in Figure 4^a

aluminum particles	onset temperature (°C) [PIR]	enthalpy (J/mg) [PIR]	onset temperature (°C) [MR]	enthalpy (J/mg) [MR]
Amorphous Al ₂ O ₃ Shell				
nonpolar	434.6	36	563	608
polar	432.0	42	557	816
Crystalline γ -Al ₂ O ₃ Shell				
nonpolar	428.8	56	550	1186
polar	426.7	64	537	1340

^aNote PIR is pre-ignition reaction and MR is main reaction. Shaded region in Figure 4 corresponds with enthalpy calculations. Onset temperature determined as the intersection of the tangents of the peak with the extrapolated data and does not correspond with shaded regions.

Figure 4 suggests that surface reactions at site I (Figure 3a) are nearly twice as likely to occur than at site IV (Figure 3c) which are nearly twice as likely to occur than site II (Figure 3b). The implication of the computed results is that the majority of surface reactions is associated with terminal hydroxyl coordinations with the octahedral terminal coordination reactions between the surface and CF₄, HF, and CH₃F in largest abundance and providing the greatest exothermic energy (from Figure 3a). The change in Gibbs free energy associated with the hydroxyl octahedral bridging coordination (site II, Figure 3b) is lower than for the hydroxyl octahedral and tetrahedral terminal coordinations (Figure 3a and 3c), and site II produces only mildly exergonic (or slightly endergonic) Gibbs free energies for the HF, CH₃F, and CF₄ reactions (Figure 3b). The hydroxyl terminal containing one octahedral and one tetrahedral Al coordination (site V) is endergonic (Figure 3d) and thus a more unlikely coordination to produce surface reactions, and Figure 3d confirms that surface reactions on this coordination are endothermic.

Because surface reactions are presumably responsible for the measured PIR behavior seen in Figure 4, examining surface reactions at elevated temperatures was of interest. Figure 3 extends the simulation results at ambient to higher temperatures. The highest temperature in the simulation is roughly 100 °C lower than the onset of the PIR (Table 2), but the trend shows that the likelihood of predicted thermodynamic behavior does not change significantly at elevated temperatures. In this way, calculations performed at room temperature are reasonable predictions of behavior at elevated temperatures.

The experimental results shown in Figure 4 and Table 2 indicate an increase in reactivity for particles that contain a crystalline γ -Al₂O₃ shell versus an amorphous Al₂O₃ shell. The more ordered nature of the crystalline shell may promote increased hydroxyl terminal bonding, specifically of site I and IV coordinations. The DFT calculations indicate these coordinations produce higher exothermic reactions with fragmented fluorine radicals such as CF₄, HF, and CH₃F from decomposing PTFE. These surface reactions are apparent as exothermic PIR in all Al powder samples (Figure 4) but are highest for Al powder with crystalline shells. The implication of this result is that changing the phase of the shell may functionalize the hydration layer toward a greater concentration of site I coordinations as a way to optimize surface exothermicity as well as main reaction exothermicity.

Experiments consistently show treatment in a polar fluid promotes greater reactivity (regardless of shell structure).

However, computations show a polar environment enhances exothermic surface reactions only for site IV coordinations but has little effect on site I. The correlation between experimental measurements of surface reaction enthalpies in Figure 4 compared to the DFT calculations in Figure 2 implies that the polar fluid treatment may promote greater site IV coordinations that contribute to a measurable increase in reaction enthalpy.

Another interesting observation from the experimental results in Table 2 is that higher enthalpies in the PIR correlate with higher enthalpies in the main reaction. In fact for both the PIR and main reaction, Figure 5 shows a linear relationship

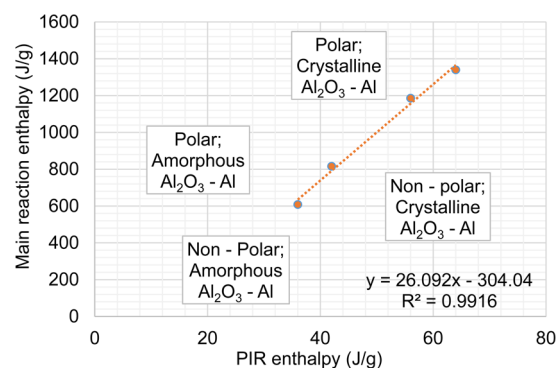


Figure 5. Main reaction enthalpy as a function of PIR enthalpy measured using DSC data (Table 2). Data points are labeled according to the carrier fluid polarity (i.e., polar or nonpolar) and according to the shell structure (amorphous or crystalline).

between both reaction enthalpies (an R^2 value of 0.99), with the crystalline shell particles producing higher enthalpies for both PIR and main reaction. The linearity predicts that ~5% of the total energy is harnessed in the PIR, while ~95% remains in the main reaction.

Two additional conclusions from the experimental results in Figure 4 and Table 2 are shown in Figure 6(a) and (b). There is a linear relationship between the onset temperature for reaction and the reaction enthalpy. In Figure 6(a), the slope of the curve indicates that reducing the onset temperature for the PIR by about 2 °C results in a 7.3 J/g increase in PIR. Similarly, reducing the onset temperature for the main reaction by about 5 °C results in an increase in main reaction by 143 J/g. The linearity seen here is consistent with the linearity seen between the PIR enthalpy and the level of hydration seen through IR intensity measurements in Figure 5 of Padhye et al.²² All of these results suggest that higher levels of hydration that may stem from surface coordinations of sites I, II, and IV result in increased surface reactions seen by higher levels of enthalpy in the PIR that promote higher levels of enthalpy in the main reaction. Tailoring the surface structure toward optimizing hydroxyl bonding that promotes surface reactions will also facilitate combustion of the main reaction.

CONCLUSIONS

Theoretical calculations and experiments reveal the key hydroxyl bonding coordinations that maximize exothermic surface reaction enthalpy and correlate with maximizing the main aluminum reaction enthalpy. Density functional theory (DFT) calculations show the most exothermic reactions occur at the terminal hydroxyl coordinations, specifically octahedral, site I, and tetrahedral, site IV, and the most exothermic

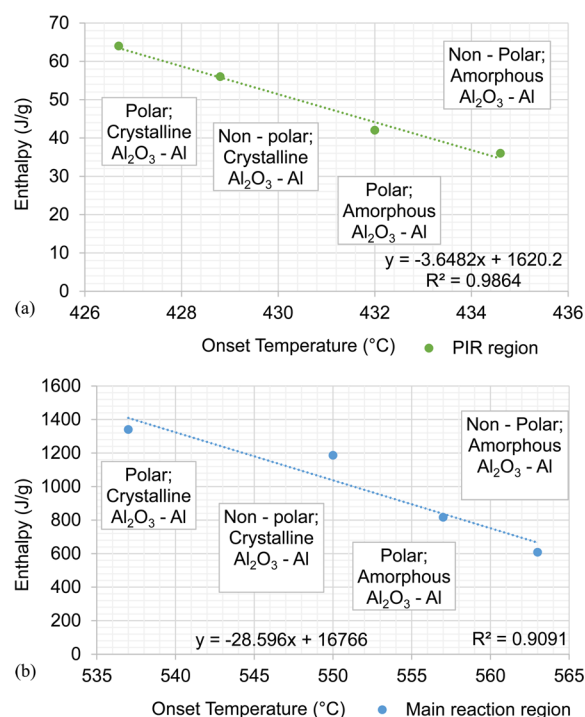


Figure 6. (a) PIR enthalpy as a function of onset temperature for reaction and (b) main reaction enthalpy as a function of onset temperature for reaction. All data measured using DSC (Table 2). Data points are labeled according to the carrier fluid polarity (i.e., polar or nonpolar) and according to the shell structure (amorphous or crystalline).

reactions for both terminal coordinations occur with $\text{CF}_4 > \text{HF} > \text{CH}_3\text{F}$. In the calculations, the differences in reaction enthalpies on the alumina surfaces for polar compared with nonpolar processing liquids are slight. Experiments were also performed that altered the naturally amorphous shell structure surrounding an aluminum core particle to crystalline $\gamma\text{-Al}_2\text{O}_3$.

Differential scanning calorimetry on amorphous compared with crystalline Al_2O_3 shell particles as well as particle mixtures combining Al with PTFE processed with either a polar or nonpolar carrier fluid were examined. Results consistently show a linear relationship between increasing preignition reaction (PIR) enthalpy and increasing main reaction enthalpy, with the crystalline shell structure optimizing the reaction enthalpy for both PIR and the main reaction over the amorphous shell structure. Also, for each shell structure, the polar processing fluid produces greater energy for both reactions. The experimental results confirm that the assumption of crystalline shell structure used in the DFT models is representative of an upper limit for the enthalpy model. The experimental results also suggest that transforming the shell toward a crystalline structure may optimize the abundance of terminal hydroxyl coordinations that are predicted to produce the highest reaction energies. These results show that optimizing energy available in a PIR will correlate with optimizing energy available in the main reaction. In this way, engineering the surface of an aluminum particle toward greater surface reactions is a way to optimize overall aluminum particle oxidation.

ASSOCIATED CONTENT

Supporting Information

The Supporting Information is available free of charge on the ACS Publications website at DOI: 10.1021/acsami.7b05372.

Transmission electron microscopy images and XRD analysis show the changes in aluminum particles post heat treatment (see Figure S1 and Figure S2, respectively). Particle size distribution was carried out to confirm the size of the PTFE used in these experiment (see Figure S3). Values for the data represented in Figures 2 and 3 have been tabulated (see Tables S1 and S2) (PDF)

AUTHOR INFORMATION

Corresponding Authors

*Phone: 806-789-1348. E-mail: adelia.aquino@univie.ac.at.

*Phone: 806-834-3733. E-mail: michelle.pantoya@ttu.edu.

ORCID

Adelia J. A. Aquino: 0000-0003-4891-6512

Michelle L. Pantoya: 0000-0003-0299-1832

Notes

The authors declare no competing financial interest.

ACKNOWLEDGMENTS

The authors are grateful for encouragement and support from the Army Research Office under grant W911NF-14-1-0250 and our program manager, Dr. Ralph Anthenien. A.J.A. Aquino is grateful for the support provided by the Robert Welch Foundation under grant number D-0005. The technical support and computer time at the Vienna Scientific Cluster (project 70544) is gratefully acknowledged. NSF Major Research Instrumentation Program Award #0421032 and Dr. Bo Zhao with College of Arts & Sciences Microscopy at TTU are acknowledged for assistance with TEM & SEM analysis, and Dr. Juliusz Warzywoda and the Materials Characterization Facility at Texas Tech University are gratefully acknowledged for XRD analysis.

REFERENCES

- (1) Gottfried, J.; Bukowski, E. Laser-shocked Energetic Materials with Metal Additives: Evaluation of Detonation Performance. *Appl. Opt.* **2017**, *56* (3), B47–B57.
- (2) Sullivan, K. T.; Zhu, C.; Duoss, E. B.; Gash, A. E.; Kolesky, D. B.; Kuntz, J. D.; Lewis, J. A.; Spadaccini, C. M. Controlling Material Reactivity Using Architecture. *Adv. Mater.* **2016**, *28* (10), 1934–1939.
- (3) Pesiri, D.; Aumann, C.; Bilger, L.; Booth, D.; Carpenter, R.; Dye, R.; O'Neill, E.; Shelton, D.; Walter, K. Industrial Scale nano-Aluminum Powder Manufacturing. *J. Pyrotech.* **2004**, *19*, 19–32.
- (4) Friedman, R.; Maček, A. Combustion Studies of Single Aluminum Particles. *Symp. (Int.) Combust., [Proc.]* **1963**, *9* (1), 703–712.
- (5) Osborne, D. T.; Pantoya, M. Effect of Al Particle Size on the Thermal Degradation of Al/Teflon Mixtures. *Combust. Sci. Technol.* **2007**, *179* (8), 1467–1480.
- (6) Pantoya, M. L.; Dean, S. W. The Influence of Alumina Passivation on nano-Al/Teflon Reactions. *Thermochim. Acta* **2009**, *493* (1–2), 109–110.
- (7) Sippel, T. R.; Son, S. F.; Groven, L. J. Altering Reactivity of Aluminum with Selective Inclusion of Polytetrafluoroethylene through Mechanical Activation. *Propellants, Explos. Propellants, Explos., Pyrotech.* **2013**, *38* (2), 286–295.

- (8) DeLisio, J. B.; Hu, X.; Wu, T.; Egan, G. C.; Young, G.; Zachariah, M. R. Probing the Reaction Mechanism of Aluminum/Poly(vinylidene fluoride) Composites. *J. Phys. Chem. B* **2016**, *120* (24), 5534–5542.
- (9) McCollum, J.; Pantoya, M. L.; Iacono, S. T. Activating Aluminum Reactivity with Fluoropolymer Coatings for Improved Energetic Composite Combustion. *ACS Appl. Mater. Interfaces* **2015**, *7* (33), 18742–18749.
- (10) McCollum, J.; Pantoya, M. L.; Iacono, S. T. Catalyzing Aluminum Particle Reactivity with a Fluorine Oligomer Surface Coating for Energy Generating Applications. *J. Fluorine Chem.* **2015**, *180*, 265–271.
- (11) King, S. W.; Davis, R. F.; Carter, R. J.; Schneider, T. P.; Nemanich, R. J. Hydrogen Desorption Kinetics for Aqueous Hydrogen Fluoride and Remote Hydrogen Plasma Processed Silicon (001) Surfaces. *J. Vac. Sci. Technol., A* **2015**, *33* (5), 05E115.
- (12) Shamiryan, D.; Baklanov, M.; Claes, M.; Boullart, W.; Paraschiv, V. Selective Removal of High-K Gate Dielectrics. *Chem. Eng. Commun.* **2009**, *196* (12), 1475–1535.
- (13) Dhungana, S.; Nguyen, T. D.; Nordell, B. J.; Caruso, A. N.; Paquette, M. M.; Chollon, G.; Lanford, W. A.; Scharfenberger, K.; Jacob, D.; King, S. W. Boron and High-K Dielectrics: Possible Fourth Etch Stop Colors for Multipattern Optical Lithography Processing. *J. Vac. Sci. Technol., A* **2017**, *35* (2), 021510.
- (14) Zivkovic, Z. D.; Pacovic, N.; Filipovic, M. Effect of AlF₃ on the Calcination of Aluminum Hydroxide. *Thermochim. Acta* **1979**, *32* (1–2), 181–188.
- (15) Deshmukh, S. S.; Kovalchuk, V. I.; Borovkov, V. Y.; d'Itri, J. L. FTIR Spectroscopic and Reaction Kinetics Study of the Interaction of CF₃CFCl₂ with Gamma-Al₂O₃. *J. Phys. Chem. B* **2000**, *104* (6), 1277–1284.
- (16) Bailey, C. L.; Mukhopadhyay, S.; Wander, A.; Searle, B. G.; Harrison, N. M. Structure and Stability of alpha-AlF₃ Surfaces. *J. Phys. Chem. C* **2009**, *113* (12), 4976–4983.
- (17) Mukhopadhyay, S.; Bailey, C. L.; Wander, A.; Searle, B. G.; Muryn, C. A.; Schroeder, S. L. M.; Lindsay, R.; Weiher, N.; Harrison, N. M. Stability of the AlF₃ (0112) Surface in H₂O and HF Environments: An Investigation Using Hybrid Density Functional Theory and Atomistic Thermodynamics. *Surf. Sci.* **2007**, *601* (18), 4433–4437.
- (18) Di Cosimo, J.; Díez, V.; Ferretti, C.; Apesteguía, C. Basic Catalysis on MgO: Generation, Characterization and Catalytic Properties of Active Sites. *Catalysis* **2014**, *26*, 1–28.
- (19) Malinowski, S.; Szczepanska, S.; Sloczynski, J. Magnesium Oxide as a Catalyst.II. Acid-Base Properties Of Magnesium Oxide Surface. *J. Catal.* **1967**, *7* (1), 68–75.
- (20) Malinowski, S.; Szczepanska, S.; Bielanski, A.; Sloczynski, J. Magnesium Oxide as a Catalyst.I. Acid-Base Properties of Magnesium Oxide Surface. *J. Catal.* **1965**, *4* (3), 324–331.
- (21) Padhye, R.; Aquino, A. J. A.; Tunega, D.; Pantoya, M. L. Effect of Polar Environments on the Aluminum Oxide Shell Surrounding Aluminum Particles: Simulations of Surface Hydroxyl Bonding and Charge. *ACS Appl. Mater. Interfaces* **2016**, *8* (22), 13926–13933.
- (22) Padhye, R.; McCollum, J.; Korzeniewski, C.; Pantoya, M. L. Examining Hydroxyl-Alumina Bonding toward Aluminum Nanoparticle Reactivity. *J. Phys. Chem. C* **2015**, *119* (47), 26547–26553.
- (23) Peri, J. A Model for the Surface of γ -Alumina. *J. Phys. Chem.* **1965**, *69* (1), 220–230.
- (24) Knozinger, H.; Ratnasamy, P. Catalytic Aluminas: Surface Models and Characterization of Surface Sites. *Catal. Rev.: Sci. Eng.* **1978**, *17* (1), 31–70.
- (25) Dirac, P. A. Quantum Mechanics of Many-Electron Systems. *Proc. R. Soc. London, Ser. A* **1929**, *123* (792), 714–733.
- (26) Slater, J. C. A Simplification of the Hartree-Fock Method. *Phys. Rev.* **1951**, *81* (3), 385–390.
- (27) Vosko, S.; Wilk, L.; Nusair, M. Accurate Spin-Dependent Electron Liquid Correlation Energies for Local Spin Density Calculations: A Critical Analysis. *Can. J. Phys.* **1980**, *58* (8), 1200–1211.
- (28) Perdew, J. P. Density-Functional Approximation for the Correlation Energy of the Inhomogeneous Electron Gas. *Phys. Rev. B: Condens. Matter Mater. Phys.* **1986**, *33* (12), 8822–8824.
- (29) Becke, A. D. Density-Functional Exchange-Energy Approximation with Correct Asymptotic-Behavior. *Phys. Rev. A: At., Mol., Opt. Phys.* **1988**, *38* (6), 3098–3100.
- (30) Schäfer, A.; Horn, H.; Ahlrichs, R. Fully Optimized Contracted Gaussian Basis Sets for Atoms Li to Kr. *J. Chem. Phys.* **1992**, *97* (4), 2571–2577.
- (31) Maryott, A. A.; Smith, E. R. Table of Dielectric Constants of Pure Liquids; DTIC Document: 1951. Circular 514.
- (32) Klamt, A.; Schuurmann, G. Cosmo - A New Approach to Dielectric Screening in Solvents with Explicit Expressions for the Screening Energy and its Gradient. *J. Chem. Soc., Perkin Trans. 2* **1993**, *5*, 799–805.
- (33) Ahlrichs, R.; Bar, M.; Haser, M.; Horn, H.; Kolmel, C. Electronic-Structure Calculations on Workstation Computers - The Program System Turbomole. *Chem. Phys. Lett.* **1989**, *162* (3), 165–169.
- (34) Firmansyah, D. A.; Sullivan, K.; Lee, K. S.; Kim, Y. H.; Zahaf, R.; Zachariah, M. R.; Lee, D. Microstructural Behavior of the Alumina Shell and Aluminum Core Before and After Melting of Aluminum Nanoparticles. *J. Phys. Chem. C* **2012**, *116* (1), 404–411.
- (35) Gesner, J.; Pantoya, M. L.; Levitas, V. I. Effect of Oxide Shell Growth on nano-Aluminum Thermite Propagation Rates. *Combust. Flame* **2012**, *159* (11), 3448–3453.